Photocatalytic Degradation of Perfluorooctanoic acid (PFOA) from wastewaters by TiO_2, In_2O_3 and Ga_2O_3 catalysts

Felipe Lopes da Silva, Tiina Laitinen, Minna Pirilä, Riitta L. Keiski and Satu Ojala*

University of Oulu, Environmental and Chemical Engineering, POB 4300, 90014 University of Oulu, Finland
*Corresponding author: satu.ojala@oulu.fi

Abstract

The aim of the work was to prepare nanosized In_2O_3 and Ga_2O_3 photocatalysts for degradation of Perfluorooctanoic acid (PFOA) in water. Their commercial references along with TiO_2 were used as a comparison basis. The characterization of the materials proved that successful preparation of cubic In_2O_3 and monoclinic ß-Ga_2O_3 were achieved via solvothermal and hydrothermal methods, respectively. The effect of different parameters such as catalyst dosage, UV light source and utilization of inorganic oxidant in PFOA treatment were evaluated. In_2O_3, photocatalyst was the most efficient in the degradation of 15 mgL^{-1} PFOA under UVB irradiation and synthetic air reaching 27% of degradation, which was 20 percentage points higher than for commercial In_2O_3. This is proposed to be partly due to significantly higher specific surface area of the self-made In_2O_3 and smaller crystallite size and partly due to more efficient absorption of UVB light compared to the other tested materials. Addition of $KBrO_3$ did not improve the activity of self-made In_2O_3.

1. Introduction

Perfluorooctanoic acid (PFOA, $C_7F_{15}COOH$) has been recently classified as an emerging persistent organic pollutant (POP) by the United States Environmental Protection Agency (U.S. EPA) [1]. It has been proposed for restriction in the European Chemicals Agency (ECHA) [2] and in October 2015, it has been submitted by the European Union to the Stockholm convention to be included in the list of POP's [3]. It belongs to the class of fully fluorinated hydrocarbons also known as perfluorcarboxylic acids (PFCAs, $C_nF_{2n+1}COOH$). PFCA's contain a characteristic carboxylic group at the terminal end of the chain of perfluorinated carbon atoms with varying length and are derived from hydrocarbons by replacing the hydrogen atoms with fluorine atoms [4, 5]. The carbon-fluorine bonds present in these molecules are very strong making PFOA extremely hydrophobic, lipophobic, as well as thermally and chemically stable with an active surface [6, 7]. Due to this characteristics PFOA has been widely utilized in industrial and commercial applications in the past six decades ranging from coatings for clothing, leather and carpets that are water, soil and stain resistant; oil resistant coatings for food packages; aviation hydraulic fluids; fire retardants (fire-fighting foams) until industrial utilization as surfactants; emulsifiers; wetting agents; additives and coatings for production of polytetrafluorethylene (PTFE) and others [8-12]. The same characteristics that makes it an important industrial and commercial constituent also makes PFOA a strong bioaccumulative and persistent compound and therefore it has often been found in the environment around the world, mainly in the water matrix, such as finished drinking water, surface water and groundwater, but also in sludge, soils, sediments, outdoor and indoor dust, polar ice caps and recently also in living organisms [8, 13-15]. The presence of PFOA in the environment is due to human activities, since it is an anthropogenic compound, and it can be either directly or indirectly released into the environment [16]. The production and use of products containing PFOA are a direct sources of PFOA reaching the environment, and its main routes of release are the effluents from wastewater treatment plants (WWTP), precipitation, runoff from contaminated soil, landfills and fire-fighting foams [8, 17]. The

indirect sources can be reaction impurities or degradation of related compounds such as fluorotelomer and perfluorosulfonamides [18]. In addition, recent studies indicate that PFOA is toxic and carcinogenic to humans and animals [6, 7]. Due to its strong bonds and persistent characteristics PFOA cannot be degraded by conventional methods usually utilized in WWTPs, and even conventional advanced oxidation processes based on titanium dioxide (TiO_2), for example, are not effective in the degradation of the compound [7, 19-21]. Due to its bioaccumulative and persistent characteristic it poses a threat to human lives and increases the need to develop new technologies capable of degrading this organic pollutant. Thus, the research on new purification possibilities, such as catalytic materials in photocatalysis and their operation parameters, need to be done in order to treat the wastewaters from industry and waters, which contain PFOA [7, 19, 20].

The goal of this research was to discover novel catalytic materials and the optimum process parameters (UV irradiation source – UVA or UVB and the catalyst loading) for the photocatalytic degradation of PFOA under milder conditions, than already reported UVC or VUV irradiation sources [12, 22-26]. Self-prepared and commercially available In_2O_3 and Ga_2O_3 were selected as the photocatalytic materials along with Aeroxide P25 TiO_2. The main aim of using the commercial analogues for In_2O_3 and Ga_2O_3 was to verify the success of the used preparation method. Aeroxide P25 was used as a reference, since it is a very, well-known, efficient photocatalyst. In addition, the effect of the inorganic oxidant was studied. The development of the new catalytic materials that are able to operate under milder conditions and with faster degradation efficiency might result in a more inexpensive treatment suitable for industries to prevent the release of such persistent pollutants and further contamination of waters and living organisms avoiding a significant source of toxicity for the environment and human beings.

2. Experimental

2.1 Materials

All the chemicals were purchased from Sigma Aldrich and used as received. Perfluorooctanoic acid (PFOA) ($C_7F_{15}COOH$ 96%), potassium periodate (KIO_4) (99.8%), potassium bromate ($KBrO_3$) (≥99.8%), gallium (III) nitrate hydrate ($Ga(NO_3)_3 \cdot xH_2O$) (99.9%), polyvinyl alcohol (PVA) (Mw = 27000), indium (III) nitrate hydrate ($In(NO_3)_3 \cdot xH_2O$) 99.9%) and 1,2 diaminopropane (≥99%) were used in catalyst preparation or in photocatalytic experiments.

2.2 Synthesis of catalysts

2.2.1 Gallium Oxide

The gallium oxide catalyst was prepared through a hydrothermal method utilizing distilled water as a solvent for the precursor gallium (III) nitrate hydrate ($Ga(NO_3)_3 \cdot xH_2O$) and assisted by polyvinyl alcohol (PVA). In a typical experiment 8.0 grams of $Ga(NO_3)_3 \cdot xH_2O$ was diluted into 80 mL of water and subsequently 0.470 grams of PVA was added to the solution, which was then kept in a magnetic stirrer for 15 minutes under 90°C before being transferred to a pressurized reactor (PARR Pressure reactor HP 4575). Based on the work developed by Shao et al. [12], hydrothermal high-pressure reaction was carried out at 200°C for a period of 8 hours, without controlling the pressure inside the reactor. After 8 hours, solution and the white precipitate were collected, and then centrifuged and washed with distilled water and ethanol five times utilizing 9000 rpm for 20 minutes each run. After the washing, the white precipitate was taken into an overnight sandbath (at 90°C) to remove impurities and evaporate water. The resulted white powder was then calcined at 700°C under nitrogen (N_2) atmosphere with 100 $mLmin^{-1}$ gas flow in the calcination oven.

2.2.2 Indium Oxide

The indium oxide catalyst was prepared through a solvothermal method utilizing ethanol and 1,2 diaminopropane as solvents for the precursor indium (III) nitrate hydrate ($In(NO_3)_3 \cdot xH_2O$). In a typical experiment 5.0 grams of $In(NO_3)_3 \cdot xH_2O$ was diluted into 60 mL of pure ethanol and subsequently 60 mL of 1,2 diaminopropane was dropped to the solution under continuous stirring. The solution was then transferred to the pressurized reactor where it was kept at 180°C for a period of 16 hours, as described in [25], without adjustment of the pressure of the reactor. The solution and the white precipitate were then collected, centrifuged and washed with distilled water and ethanol five times utilizing 9 000 rpm for 20 minutes each run. After the washing the white precipitate was taken into an overnight sandbath (at 90°C) to remove impurities and for drying. The white precipitate was then calcined at 500°C under 100 $mLmin^{-1}$ flow of Synthetic Air (O_2/N_2).

2.3 Characterisation of Catalysts

The equipment utilized for calculation of the *specific surface area and pore volume (BET-BJH)*, was a Micrometrics ASAP 2020. The results were achieved by utilizing Nitrogen (N_2) adsorption-desorption isotherms at 196°C (77 K). Prior the analysis, the samples were pre-treated at 300°C under vacuum for 2 hours to eliminate adsorbed compounds. A Timegated® 532 *Raman* instrument was utilized to obtain the Raman spectra of the prepared catalysts. The Timegated® Raman is equipped with sub-nanosecond (100 ps) laser excitation source (532 nm) coupled with time-gated single photon counting array detector. Such arrangement is capable of suppressing fluorescence interference. *Thermogravimetric analysis* was performed in a Netzch STA 449F3 Jupiter for the precursors of the catalysts prepared ($In(OH)_2$ and GaO(OH)). The analysis was performed with approximately 20 mg of each sample in a N_2/O_2 atmosphere and it was set for a range of 20-1200°C with a heating ramp of 5°C per minute for the gallium compound and the range of 20-1000°C with a heating ramp of 5°C for Indium. The equipment utilized for the *XRD analysis* was a SIEMENS Diffractometer D5000.

The samples were analyzed using $10° \leq 2\,\theta \leq 85°$ scale with 0.02° step and a step time of 1 second with Cu K_α radiation (λ = 1.5406 Å). The *Field Emission Scanning Electron Microscope* (FESEM) utilized was a ZEISS SIGMA FESEM. The samples were coated with a carbon layer to avoid accumulation of charge before being inserted into the FESEM and the acceleration voltage selected was 5.0 kV. The *band-gap measurements* were done with Varian Cary 5000 UV-vis-NIR spectrophotometer with integrating sphere. Two different sample holder were used, the tailor-made vertical sample holder that allowed the direct measurement from powder-form sample was prepared by VTT Finland. For the conventional sample holder the catalysts were pressed as self-supporting wafers. The spectra were collected from about 250 nm to 650 nm wavelength range. The *XPS measurements* were done with Thermo Fisher Scientific ESCALAB 250Xi X-ray photoelectron spectroscopy (XPS) system equipped with the Al K_α X-ray source =1486.7 eV. The X-ray source operated at 10 mA and 12 kV. The static charge of the samples was corrected by referencing all binding energies (BE) to the C1s peak (BE= 284.8 eV).

2.4 Photocalytic experiments

The photocatalytic experiments were performed in a 1 litre annular type vertical batch Teflon reactor (Figure 1) with an inner glass cylinder and a quartz inner tube, where the UV light source lamp (UVA Philips PL-L 36W, 350-360 nm and UVB Philips PL-L Hg - 36W/01/4P) was placed. The irradiance of the lamp was measured with a Delta Ohm Photo-radiometer HD 2302.0 in the annulus of the reactor and it was 52 Wm^{-2} for the UVA and 12 Wm^{-2} for the UVB. Synthetic air with a constant rate of 0.1 $Lmin^{-1}$ was fed to the reactor during the experiments. The reactor was placed on top of a magnetic stirrer Heidolph MR 3000 that was kept at 250 rpm to allow a good agitation of the solution. Temperature was kept at 25°C ± 1°C monitored through a thermocouple thermometer Delta Ohm HD 2128.1 and adjusted with a cool water flow circulating through a steel coil inside the reactor, regulated with a flow-meter. The PFOA solution was prepared by dissolving 15 mg of PFOA into 0.5 L of

distilled water and it was kept stirring overnight to ensure proper dilution. Then it was poured into the reactor, where the catalysts were added on. The pH of the solution was monitored, but never adjusted. The experiments were conducted for 210 minutes, where in the initial 30 minutes the light source was off (dark period) for reaching the adsorption-desorption equilibrium, and for the remaining 180 minutes the UV light source was turned on. The 5 mL samples were collected through a sampling port utilizing a pipette, and afterwards filtered through a syringe disc filter of 0.22 μL (Minisart 16555-Q). Mass Spectrometry (Waters Synapt G1) was utilized as analytical method in TOF mode with electrospray ionization (ES) with a capillary voltage of 3.0 kV and 5μL injection volume. The commercially available catalysts (In_2O_3 and Ga_2O_3 from Sigma Aldrich and Aeroxide P25 TiO_2 as a reference catalyst) were utilized to achieve the optimum conditions for PFOA degradation and then the performance of the self-made catalysts were evaluated. Additionally, experiments where the inorganic oxidants, $KBrO_3$ (0.5 g) and KIO_4 (0.45 g) were added to the PFOA (15 mgL^{-1}) solution to discover their impacts on the degradation were performed.

Figure 1

3 Results

3.1 Characterisation

3.1.1 Thermogravimetric analysis (TGA)

The TGA analysis results are shown in Figures 2a & b. Based on the curves obtained, it is clear that the calcination temperature selected was high enough, as gallium hydroxide loss of mass happens at around 410°C and the temperature selected for calcination was 700°C while with indium hydroxide,

the major loss of mass took place between 200-300°C and the calcination temperature used was 500°C.

Figure 2

According to the stoichiometry of the reaction $2In(OH)_3 \rightarrow In_2O_3 + 3H_2O$ the mass loss should be equivalent to 16.3% during the TGA, the difference in the values is probably due to the impurities and other compounds that remained in the catalyst after solvothermal preparation. For the reaction $2GaO(OH) \rightarrow Ga_2O_3 + H_2O$ the mass loss expected was 9.6% which was very close to the result found.

3.1.2 Specific Surface Area (S_{BET}), pore volume and size (BET/BJH) and Particle size fraction

The nitrogen isotherm curves are shown for the commercial and experimentally prepared gallium oxide in Figure 3a & c and for indium oxide in Figure 3b & d. All catalysts analysed presented a Type IV curve according the International Union of Pure and Applied Chemistry (IUPAC) classification, and it is in accordance with several results published earlier [6, 12, 24, 25]. Type IV isotherm is characteristic for mesoporous materials (2nm (20 Å) ≤ pore size ≤ 50nm (500 Å)), with a presence of capillary condensation in the pores. As the capillary condensation in the mesopores is not reversible a hysteresis loop is observed. Commercial gallium presented a hysteresis loop of the type H_1, which presents nearly parallel and vertical branches of adsorption and desorption and it is characteristic of material having a very narrow distribution of mesopores. For the self-made catalyst the hysteresis loop was closer to a type H_2 indicating the presence of interconnected mesopores, which can be confirmed from the FESEM images later on.

The self-made indium catalyst presented also a small hysteresis loop, classified as an H_3 hysteresis loop. The H_3 hysteresis loop is a characteristic for aggregated particles, in which the capillary condensation occurs in pores that are formed between the particles forming a non-rigid structure. The aggregation of the particles can also be later confirmed by the electron microscopy images.

Information about the pore volume and distribution are shown in Figures 3 e & g for gallium catalysts and in 3 f & h for indium catalysts. From the results it is possible to observe that the self-made gallium catalyst have higher amount of pores with smaller diameter in the range of 25 - 70 Å, while the commercial one presents higher amounts of pores in the range of 60 - 250 Å. This is in accordance with the higher surface area found for the self-made gallium catalyst of 15 m^2g^{-1} versus 8 m^2g^{-1} for the commercial one. For the commercial indium catalyst we can see the presence of pores in the range of 20 - 40 Å and a higher amount of pores above the 200 Å pore diameter, which is believed to be caused by the aggregation of smaller particles that generate pores between them. This can be confirmed by the FESEM images later on as well. For the self-made indium catalyst, due to the small particle size, the pore distribution curve combines the smaller pores present in the particles and the aggregation of the particles which generates pores among them indicating pores in a range of 20 – 1000 Å. The FESEM images show the small particle size that triggers this kind of behaviour on the pore-size distribution curves and is confirmed by the H_3 hysteresis loop found on the nitrogen isotherm curve. The BET surface area for the commercial indium was 4 m^2g^{-1}, while the self-made catalyst presented a much higher value of 70 m^2g^{-1}.

Figure 3

The particle size fractions were also calculated and can be seen from Table 1, which indicates that the indium catalysts had smaller particles with most of the particles being smaller than 45 µm while for the gallium catalysts the majority of particles were in the range between 250 µm – 100 µm.

Table 1

3.1.3 Raman spectroscopy

Figure 4.a shows the Raman spectra for the self-made and commercial gallium oxide. The peaks observed for both at 140, 167, 197, 318, 344, 413, 470, 628, 653 and 765 cm^{-1} are well in accordance with the peaks reported for monoclinic gallium oxide nanobelts by Khan et al. [28]. The Raman active modes of monoclinic gallium oxide can be divided in three general groups: low frequency liberation and translation of tetrahedral-octahedral chains visible below 200 cm^{-1}, mid-frequency deformation of Ga_2O_6 between 310-480 cm^{-1} and high-frequency stretching and bending of GaO_4 between 500-770 cm^{-1} [29]. Rao et al. [29] have also presented expected bulk frequencies for gallium oxide that are 144, 169, 200, 317, 344, 416, 472, 629, 654 and 767 cm^{-1}. Comparison of our data to these reported frequencies, we observe that some of the peaks are slightly red-sifted indicating the presence of defects in the material. The peak observed for the self-made catalyst at 280 cm^{-1}, is not expected for Ga_2O_3 bulk and neither exist in Raman active modes calculated for monoclinic ß-Ga_2O_3 by Local Density Approximation (LDA) reported in ref [29]. However, Zhao and Frost [30] have investigated α-gallium oxyhydride and β-gallium oxide nanorods with Raman spectroscopy. They suggested that the peaks observed at 261, 275, 433 and 522 cm^{-1} are related to the OH group of α-GaO(OH), when polyethylene oxide was used as a surfactant. After calcination at 900°C for 2 hours, these peaks disappeared and only very small peaks at 261 and 275 cm^{-1} remained visible. This allows us to consider the unresolved peak in our case at 280 cm^{-1} could be related to OH vibration since the used calcination temperature in our case was 700°C and the preparation method used was hydrothermal processing of gallium nitrate precursor in presence of polyvinyl alcohol as a surfactant. During the preparation $Ga(NO_3)_3 \cdot xH_2O$ reacts to GaO(OH), which is then transformed to Ga_2O_3 by calcination. Furthermore, the resolution of the used Raman device is about 10 cm^{-1}.

The peaks in the Raman shift for the indium oxide (Figure 4.b) at 131, 302, 361, 495 and 629 cm^{-1} are in accordance with the information found in literature for indium oxide [31, 32]. Gan et al. [31] have studied promoting effects of oxygen vacancies in photochemical performance of In_2O_3 nanocubes. In Raman spectrum the vibration occurring at 367 cm^{-1} is related to In-O-In stretching vibration, but also represents the oxygen vacancies in the indium oxide structure. Upon heating the material, the intensity of the peak decreases indicating the reduction in number of oxygen vacancies [30]. In our case, we observe a peak at 361 cm^{-1} for both the commercial and self-made indium oxide, which could indicate the presence of the oxygen vacancies in both the materials. It has been reported before by e.g. Nakamura *et al*. [33] that the presence of oxygen vacancies in TiO_2 improve the photocatalytic properties of the material and shift the activity towards visible light region. However, the calcination temperature used in our case was 500°C, which is higher than used by Gan *et al*. [31] and we would expect that the amounts of oxygen vacancies in our sample is reduced compared to the In_2O_3 calcined at lower temperature (e.g. 250°C).

Figure 4

3.1.4 X-ray Diffraction (XRD)

The diffraction patterns obtained for the commercial and self-prepared catalysts are shown in Figures 5 a, b.

Figure 5

Based on the JCPDS library [01-076-0573 (*) and 00-006-0523 (o) for both commercial and self-made Ga_2O_3] we can observe presence of monoclinic β-Ga_2O_3. This is well in accordance with the

Raman results that indicated the presence of monoclinic β-Ga_2O_3. In the case of indium oxide, JCPDS files 01-089-4595 (o) resolved all the peaks of commercial In_2O_3 showing the presence of cubic In_2O_3. For self-made indium oxide JCPDS files 00-006-0416 & 00-001-0929 (*) and 01-072-0683 (♦) were observed indicating also the presence of cubic In_2O_3. The crystallite size was calculated utilizing the Scherrer's equation (eq. 1) for the catalysts.

$$Dp = \frac{K\lambda}{\beta \cos\theta} \quad (1)$$

Where D_p is the average crystallite size in nm, K the Scherrer's constant, β is width of the peak broadening at half maximum in radians, λ is the wavelength of X-ray radiation source (nm) and θ is the Bragg's angle. The values found for commercial and self-made indium oxide were 120 and 20 nm, respectively, and commercial and self-made gallium oxide 50 and 40 nm in that order. The crystallites of the self-prepared materials were thus smaller than in the commercial ones. This is, however, a rough estimation for comparison purposes, since Scherrer's equation does not allow us to evaluate the XRD data accurately due to the broad range of small crystallites. As FESEM images later show, the crystallinity of the materials is quite complicated and more sophisticated methods such as Rietveld refinement should be used.

3.1.5 Scanning Electron Microscopy (SEM)

Figure 6 shows the FESEM images obtained when comparing the commercial and the experimental catalysts

Figure 6.

From the images obtained it is visible that the particle sizes of the self-made Ga_2O_3 are smaller than the commercial one, which is in accordance with the BET results showing higher specific surface area that facilitates the adsorption of the pollutants onto the surface of the catalyst and should improve its performance as a photocatalyst. Furthermore, the XRD results showed smaller crystallites for self-made Ga_2O_3. Separate rod-shaped crystals are seen for Ga_2O_3 while in the case of In_2O_3 FESEM analysis shows the presence of less structured aggregated particles that were also expected based on BET-BJH analysis. The existence of rod-shaped Ga_2O_3 is in accordance with Raman results where the presence of nano-belts was speculated. The FESEM image also shows somewhat rougher surface structure of self-made In_2O_3 when compared to commercial In_2O_3, which could explain also the significantly higher specific surface area of the self-made indium oxide.

3.1.6 XPS analysis

The Fig. 7 shows the XPS spectra of commercial and self-made Ga_2O_3. Ga 3d peaks at 22.84–23.27 eV, 21.19 eV and 19.97–20.35 eV corresponding to the peak of Ga_2O_3 (Ga^{3+}), Ga_2O (Ga^{+}), and metallic Ga (Ga^{0}), respectively. The observed values were higher than the values which have been presented typically in the literature (gallium oxide between 20 to 21.5 eV, gallium suboxide 19-20 eV and metallic gallium 18-19 eV) [34-36]. In the self-made Ga_2O_3 the peak at 26.25 eV can be attributed to binding energy of O2s [36-37]. In the self-made sample peak position was 0.38–0.43 eV higher than in the commercial catalyst. The portion of Ga^{3+} was 1.4 % lower in the commercial Ga_2O_3 catalyst than in self-made Ga_2O_3 catalyst. The ratio of chemisorbed oxygen to total oxygen was considerably higher (23.8%) in the self-made Ga_2O_3.

Figure 7

The deconvolution of the O1s spectra revealed three peaks for commercial Ga_2O_3 catalysts and two peaks for self-made Ga_2O_3 catalyst. The main peak in the O1s spectrum was located at 529.99–530.43 eV, which corresponds to lattice oxygen (O_α) [38] The second peak was located at 530.58-531.99 eV corresponding to chemisorbed oxygen (O_β) [38]. The third peak in the oxygen O1s spectrum of commercial Ga_2O_3 located 533.58 eV could be attributed to oxygen impurities, such as hydroxyl groups (O_θ) [39].

XPS spectra of commercial and self-made In_2O_3 are presented in Fig. 8. In 3d peaks at around 444.1 eV and 451.6 eV correspond to the In $3d_{5/2}$ and $3d_{3/2}$ peak of In_2O_3, respectively. Nearly the same values have been reported in the literature [26, 39-40]. In 3d peaks at around 443.8 eV and 451.4 eV relate to the In $3d_{5/2}$ and $3d_{3/2}$ peaks of metallic In^0, respectively. [37, 39] Positions of binding energies (BE) are almost the same for commercial and self-made In_2O_3 catalysts (BE shift 0.13–0.22). The portion of In^{3+} was 3.8 % higher in the commercial In_2O_3 catalyst than in the self-made In_2O_3 catalyst.

Figure 8

The deconvolution of the O1s spectra (Fig 8b) revealed two peaks for commercial and self-made In_2O_3 catalysts. The main peak in the O1s spectrum was located at 529.43–529.55 eV, which corresponds to lattice oxygen (O_α) [38]. The second peak was located at 531.19 eV, which is related to chemisorbed oxygen (O_β) [38]. The ratio of chemisorbed oxygen to total oxygen was 1.5% higher on the commercial In_2O_3.

Figure 8

BE values, BE shift, portion of In^{3+} and Ga^{3+}, and ratio of chemisorbed and total oxygen are presented in Tables 1 and 2. The ratio and portion of In^{3+} and Ga^{3+} oxidation states were calculated from areas of each atoms (presented XPS Figs 7 and 8).

Table 2

Table 3

3.2 Photocatalytic degradation of PFOA

To verify the level of photocatalytic effect, adsorption and photolysis experiments were carried out for PFOA removal. The degradation percentage was calculated by utilizing Equation 2:

$$\text{Degradation (\%)} = \frac{[C_0]-[C]}{[C_0]} \quad (2)$$

Where [C] is the concentration (mgL^{-1}) of PFOA at a given time and [C_0] is the initial concentration (mgL^{-1}) of PFOA in the sample.

Photolysis experiments utilizing UVA and UVB light sources represented close to 10% degradation of PFOA without addition of catalysts with UVB, while UVA showed irrelevant results. The effect of the UV light source on each commercial catalyst (0.2 gL^{-1}) was also tested aiming to identify the possible best light source for each catalyst tested and the results lead to utilisation of higher energy UVB irradiation in the proceeding experiments. Adsorption of PFOA was carried out for the commercial catalysts without light irradiation for 180 minutes. The results varied from 6-7% being almost the same for the catalysts studied.

Experiments were done to achieve the optimum catalyst dosage, by utilizing the commercial catalysts. According to the results presented in Figure 9, TiO_2 showed a better performance with the maximum

catalyst loading tested, which was 1.0 gL^{-1}, while the commercial indium catalyst reached a higher degradation degree with a lower loading of 0.2 gL^{-1}. For the commercial gallium oxide the difference between the loading of 0.2 and 0.5 gL^{-1} was not that significant (less than 1%). When considering that more than double amount of catalyst was used in the latter case and what the impacts of this would be on scaling up the process (increase in costs and the need of bigger amounts of expensive catalyst), the decision was to carry on the experiments utilizing 0.2 gL^{-1} for Ga_2O_3 as well.

Figure 9

Figure 10 presents the results of PFOA degradation with all the catalysts (commercial and self-made) when using previously defined optimal conditions (UVB light source and each catalyst optimum dosage). The experiments were carried out for 210 minutes where for 30 minutes the solution was kept in the dark (absorption) and afterwards the UV light source was turned on (180 minutes). The degradation presented in Figure 10 is from the samples taken at the end of the experiment (after the 210 minutes).

Figure 10.

According to these results the catalyst that showed the highest degradation of PFOA at the end of the experiment was the self-made indium oxide reaching 27% of degradation of the pollutant, followed by the TiO_2, commercial Ga_2O_3, commercial In_2O_3 and self-made Ga_2O_3. The higher activity of self-made In_2O_3 can possibly be related to its significantly higher specific surface area compared to the other catalysts tested.

The bandgap values measured were 2.76 eV for commercial indium, 2.26 eV for self-made indium and 4.14 eV for commercial gallium, which are somewhat in accordance with what has been found in literature [12, 19, 24]. These values confirm that In_2O_3, has a lower bandgap energy, which allows a higher absorption of light when utilizing UVB as a light source and therefore should present a higher degradation result. Gallium, on the other hand, with its higher bandgap value has a lower absorption of light when moving towards the visible light region, which help understanding the lower degradation values of the gallium catalysts. The bandgap measurements in the case of self-made Ga_2O_3 did not give us conclusive results, most probably due to higher absorption caused by the colour of the sample. According to previous results published [6, 7, 12, 19, 24-26], commercial In_2O_3 and Ga_2O_3 when utilizing UVC as a light source, reached 80%, and 40% degradation of PFOA molecule, respectively, in less than 3 hours, while with TiO_2 catalyst under UVA irradiation, degradation close to 31% of the total PFOA present in the solution was observed. In these studies much lower concentration of PFOA was used when compared to our experiments and very often instead of air, pure oxygen was used as the oxidant. Those differences in addition to the different light source (UVB instead of UVC) explains in general the lower degradation results observed in our studies as we are aiming to milder conditions of the reaction that can be applied in a larger scale process.

It is believed that the higher degradation rate of PFOA in the presence of In_2O_3 catalyst is due to its interaction with the PFOA molecule. As described by [6, 12, 25], the coordination of PFOA onto the surface of In_2O_3 and Ga_2O_3 occurs on a bidentate (or bridging) form that causes a degradation of the compound based on the direct hole oxidation happening on the surface of the catalyst. On TiO_2, the binding form is unidentate meaning that the oxidation happens mainly due to the indirect hole from $OH\cdot$ radicals generated by oxidation of H_2O or OH^- molecules present in the solution, and which happens in a slower pace than the direct hole oxidation process.

Nonetheless, in this study, TiO_2 reported a higher degradation rate than gallium oxide and even higher than commercial indium oxide. The XRD results showed smaller crystallite size and FESEM analysis showed somewhat smaller particle size for the self-made In_2O_3, which is in accordance with the higher specific surface area of the self-made catalyst, and which would partly explain the higher efficiency of self-made In_2O_3. The specific surface area of P25 Aeroxide TiO_2 is typically on the level of 50 m^2g^{-1}, which could explain its second position in the efficiency of PFOA degradation ranking. Exception to this justification is seen with self-made Ga_2O_3 that have 15 m^2g^{-1} specific surface area, but exhibits lowest degradation efficiency of PFOA among the tested catalytic materials. It seems that the availability of active surface area is not the most important property of the catalyst explaining the observed differences in the activities.

Li *et al.* [26] has proposed that the $O_\beta/(O_\alpha+O_\beta+O_\theta)$ ratio calculated in Table 3 provides information about the oxygen vacancies level of the material, and how it can possibly influence on the photocatalytic reaction by separating the photogenerated electron-hole pairs. Based on the calculations it would be expected that the self-made gallium oxide presents a higher degradation rate than its commercial pair, since it has a higher $O_\beta/(O_\alpha+O_\beta+O_\theta)$ ratio, but that did not happen possibly due to the higher bandgap value of the self-made one. The ratio for the indium catalysts was almost the same for the self-made and commercial and therefore cannot explain the higher activity of self-made In_2O_3.

Previous studies [6, 12, 15, 19, 20, 41] have utilized liquid chromatography for analysis of the intermediates, which has confirmed the presence of long and short chains of PFCA's in the solution during the degradation. The presence of the longer chain PFCA's is usually higher at the beginning of the process, and then reduce gradually while the shorter chains appear when approaching the end of the reaction. This indicates that the degradation happens in a step wise manner through a loss of a CF_2 unit at a time. The CF_2 unit later dissociates into CO_2 and F^-. Therefore a considerable amount of

intermediates is generated during the PFCA degradation. The intermediates found are perfluoroheptanoic acid ($C_6F_{13}COOH$), perfluorohexanoic acid ($C_5F_{11}COOH$), perfluoropentanoic acid (C_4F_9COOH), perfluorobutanoic acid (C_3F_7COOH), pentafluoropropanoic acid (C_2F_5COOH) and trifluoroacetic acid (CF_3COOH). No general acceptance on the mechanism of the reaction has been reached yet although many different theories such as the photo-redox or the β-scission pathway have been suggested [15]. Many factors can influence the proposed reaction pathway such as pH of the solution that can alter the behaviour of the PFOA. Furthermore, the presence of the F^- in the solution can induce catalyst deactivation that should be studied in more detail.

3.3 Effect of Inorganic Oxidants

In order to avoid electron hole recombination in a photocatalytic reaction, molecular oxygen from inorganic oxidants can be used as electron acceptor and also provide other oxidizing species that can help to accelerate the reaction [43]. Several different inorganic oxidants were tested for the degradation of pentafluorobenzoic acid in ref. [43] where IO_4^- and BrO_3^- were the most successful ones, therefore, the decision of utilizing these two inorganic oxidants in this study was made.

As stated by Ravichandran et al. in ref. [43], when IO_4^- ions are irradiated by UV light it generates highly reactive intermediates (eq. 1, 2 and 3), which increase the number of free radicals in the solution and thus enhance the degradation of organic pollutants.

$$IO_4\cdot^- + h\nu \longrightarrow IO_3\cdot + O\cdot^- \quad (1)$$

$$O\cdot^- + H^+ \longrightarrow OH\cdot \quad (2)$$

$$OH\cdot + IO_4^- \longrightarrow OH^- + IO_4\cdot \quad (3)$$

Thus, the addition of oxidants increase the charge separation due to acceptance of electrons from conduction band by these compounds (eq. 4):

$$BrO_3^- + 6e_{CB}^- + 6H^+ \longrightarrow Br^- + 3H_2O \quad (4)$$

The addition of the inorganic oxidants was studied for the PFOA degradation under UVB light. Potassium bromate presented the highest degradation reaching close to 20% of degradation of PFOA from the initial solution as illustrated in Figure 11.

Figure 11

Since potassium bromate was proven to be more efficient than potassium periodate, the further experiments were performed with the addition $KBrO_3$. Figure 12 shows the results of the experiments carried out with and without the presence of inorganic oxidant and the catalysts.

Figure 12

The inorganic oxidant increased the degradation percentage in three of the five tests performed (commercial In_2O_3, commercial and self-made Ga_2O_3). For the self-prepared indium oxide and titanium dioxide the result was opposite. This was unexpected, since the presence of the inorganic oxidant should inhibit the electron hole recombination by accepting an electron from the conduction band and thereby improve the degradation. A possible explanation for this can be a higher turbidity of the solution which does not allow the absorption of photons by the photocatalyst. According to previous study, [43] TiO_2 has reported to have higher degradation rates in the presence of $KBrO_3$. Further studies on the amount of inorganic oxidants to be added to the solution and more detailed studies could help to understand better this relationship.

4. Conclusion

The aim of the current study was to investigate PFOA degradation, since it is present in the wastewaters, known to be a very recalcitrant compound and it is difficult to treat with the current water treatment methods. In this work we proposed the photocatalytic PFOA degradation over rather scarcely studied In_2O_3 and Ga_2O_3 photocatalysts as an alternative treatment method. The results were compared with PFOA degradation over TiO_2, Aeroxide P25, which is very well-known and efficient photocatalyst. As a result, we were able to synthesize successfully nanosized cubic indium oxide and nanosized monoclinic ß-gallium oxide via solvothermal and hydrothermal methods, respectively. The success of the synthesis was proven by several characterization methods and comparison of results to commercial analogues. The PFOA degradation experiment under UVB irradiation, using air as an oxidant and 15 mgL^{-1} concentration of PFOA showed maximum 27% efficiency over self-prepared In_2O_3, which was 20 percentage points higher than with analogous commercial In_2O_3. The specific surface area of self-made indium oxide was observed to be significantly higher than that of the commercial one in addition to a smaller crystallite size calculated from XRD results. However, this is not the only characteristic that explains the differences between the catalyst activities, since similar result was not observed with gallium oxide. More likely and as the band gap measurements showed, indium oxide has higher absorption of light when moving towards visible light that could explain the better performance. More detailed study on recombination of electrons with holes on the catalyst surface should be done to explain better the degradation mechanism. Addition of $KBrO_3$ did not improve the performance of self-prepared In_2O_3 even though significant improvement were observed with commercial In_2O_3 and Ga_2O_3 as well as self-made Ga_2O_3. In general, our results show the good potential of nanosized In_2O_3 photocatalyst in PFOA degradation, however, efforts are still needed to improve its performance further, especially aiming at milder operation parameters for the reaction.

References

[1] United States Environmental Protection Agency (EPA) (2014) [Accessed 21 March 2016] Available from: http://nepis.epa.gov/Exe/ZyPURL.cgi?Dockey=P100LTG6.txt

[2] European Chemicals Agency (2014) [Accessed 21 March 2016] Available from: http://echa.europa.eu/documents/10162/e9cddee6-3164-473d-b590-8fcf9caa50e7.

[3] Stockholm Convention (2016) [Accessed 8 March 2016]. Available from: http://chm.pops.int/Home/tabid/2121/Default.aspx

[4] Panchangam S, Lin A, Shaik K, Lin C (2009) Chemosphere 77: 242-248.

[5] Thi L, Do H, Lee Y, Lo S. (2013) Chem. Eng. J. 221: 258-263.

[6] Li Z, Zhang P, Li J, Shao T, Li X (2012) Appl. Catal. B Environ. 125: 350-357.

[7] Chen M-J, Lo S-L, Lee Y-C, Huang C-C (2015) J. Hazard Mater 288: 168-175.

[8] Buck R, Franklin J, Berger U, Conder J, Cousins I, Voogt P, Jensen A, Kannan K, Mabury S & van Leeuwen, S (2011) Integr. Environ. Assess. Manage. 7: 513-541.

[9] Chen Y-C, Lo S-L, Kuo J (2011) Water Res. 45: 4131-4140.

[10] Lindstrom A, Strynar M, Libelo E (2011) Environ. Sci. Technol. 45: 7954-7961.

[11] Post G, Cohn P, Cooper K (2012) Environ. Res. 116: 93-117.

[12] Shao T, Zhang P, Jin L, Li Z (2013) Appl. Catal., B 142–143: 654-661.

[13] Cornelis C, D'Hollander W, Roosens L, Covaci A, Smolders R, Van Den Heuvel R, Govarts E, Van Campenhout K, Reynders H, Bervoets L (2012) Chemosphere 86: 308-314.

[14] Johansson J, Berger U, Vestergren R, Cousins I, Bignert A, Glynn A, Darneurd P (2014) Environ. Pollut. 188: 102-108.

[15] Sansotera M, Persico F, Rizzi V, Panzeri W, Pirola C, Bianchi C, Mele A, Navarrini W (2015) J. Fluorine Chem. 179: 159-168.

[16] European Food Safety Authority- EFSA (2008) The EFSA Journal 653: 1-131.

[17] Ahrens L, Felizeter S, Ebinghaus R (2009) Chemosphere 76: 179-184.

[18] Prevedouros K, Cousins I, Buck R, Korzeniowski S (2006) Environ. Sci. Technol. 40: 32-44.

[19] Li Z, Zhang P, Li J, Shao T, Jin L (2013) J. Photochem. Photobiol., A 271: 111-116.

[20] Cheng J-H, Liang X-Y, Yang S-W, Hu Y-Y (2014) Chem. Eng. J. 239: 242-249.

[21] Estrellan C, Salim C, Hinode H (2010) J. Hazard. Mater. 179: 79-83.

[22] Chen J, Zhang P, Liu J (2007) J. Environ. Sci. 19: 387-390.

[23] Cao M, Wang B, Yu, H, Wang L, Yuan S, Chen J (2010) J. Hazard. Mat. 179: 1143-1146.

[24] Li X, Zhang P, Jin L, Shao T, Li Z, Cao J (2012) Environ. Sci. Technol. 46: 5528-5534

[25] Li Z, Zhang P, Li J, Shao T, Wang J, Jin L, Li X (2013) J. Hazard. Mat. 260: 40-46.

[26] Li Z, Zhang P, Li J, Shao T, Wang J, Jin L (2014) Catal. Commun. 43: 42-46.

550 [27] Pirilä M (2015) Adsorption and photocatalysis in water treatment: Active, abundant and
551 inexpensive materials and methods. ACTA Univ. Oul. C 522, Oulu.

552 [28] Khan A, Khan S, Jadwisienczak W, Kordesch M (2009) Sci. Adv. Mat. 1: 236-240

553 [29] Rao R, Rao A, Xu B, Dong J, Sharma S, Sunkara M (2005) J. Appl. Phys. 98: 094312

554 [30] Zhao Y, Frost R (2008) J. Raman Spectrosc. 39: 1494-1501.

555 [31] Gan J, Lu X, Wu J, Xie S, Zhai T, Yu M, Zhang Z, Mao Y, Wang S, Shen Y, Tong Y (2012)
556 Sci. Rep. 3: 1021.

557 [32] Chong S, Azizan S, Chan K, Nguyen H, Chiu W, Aspanut Z, Dee C, Rahman S (2013)
558 Nanoscale Res. Lett. 8: 1-9.

559 [33] Nakamura I, Negishi N, Kutsuna S, Ihara T, Sugihara S, Takeuchi K (2000) J Mol Cat A-Chem
560 161: 205-212.

561 [34] Cademartiri L, Martin M, Thuo M, Nijhuis C, Reus W, Tricard S, Barber J, Sodhi R,
562 Brodersen P, KimC, Chiechi R, Whitesides G (2012) J. Phys. Chem. C 116: 10848−10860.

563 [35] Carli R, Bianchi C (1994) Appl. Surf. Sci. 74: 99–102.

564 [36] Diaz Y, Melo L, Mediavilla M, Albornaz A, Brito J, Albornoza A (2004) J Mol Cat A-Chem
565 227: 7–15.

566 [37] Lin T, Zhang H, Sun R, Duan Y, Lin N, Ma X (2015) J Alloy Compd 644: 398–403.

567 [38] Väliheikki A, Kolli T, Huuhtanen M, Maunula T, Keiski, R-L (2015) Top Catal 58: 1002 –
568 1011.

569 [39] Nguyen M-C., Jang M, Lee D-H, Bang H-J, Lee M, Jeong J, Yang H, Choi R (2016) Scientific
570 Reports 6: 25079.

571 [40] Dong C, Liu X, Han B, Deng S, Xiao X, Wang Y (2016) Sensor Actuat B-Chem 224: 193–
572 200.

573 [41] Song C, Chen P, Wang C, Zhu L (2012), Chemosphere 86: 853-859.

574 [42] Ravichandran L, Selvam K, Krishnakumar B, Swaminathan M (2009) J. of Hazard. Mat. 167:
575 763-769.

Figure captions:

Figure 1 - Experimental set-up for photocatalytic PFOA degradation [27].

Figure 2 - TGA curve for a) GaOOH and b) $In(OH)_2$

Figure 3 - N_2 adsorption-desorption isotherm curves and pore size distribution of the Ga_2O_3: a & e commercial and c & g experimental; and of the In_2O_3: b & f commercial and d & h experimental.

Figure 4 - Raman shift for self-made and commercial: a) gallium oxide and b) indium oxide.

Figure 5 - XRD patterns of self-made and commercial: a) gallium oxide (JCPDS library 01-076-0573 (*) and 00-006-0523 (o)) and b) indium oxide (JCPDS files 01-089-4595 (o); 00-006-0416 & 00-001-0929 (*) and 01-072-0683 (♦))

Figure 6 - FESEM images of: a) Commercial and b) self-made Ga_2O_3; c) commercial and d) self-made In_2O_3

Figure 7 - XPS spectra of self-made and commercial Ga_2O_3: a) Ga 3d and b) O1s

Figure 8 - XPS spectra of self-made and commercial In_2O_3: a) In 3d and b) O1s

Figure 9 - Degradation of PFOA over 180 minutes of UVB irradiation with different catalyst dosages for commercial TiO_2, commercial In_2O_3 and commercial Ga_2O_3.

Figure 10 – Photocatalytic degradation of PFOA after 180 minutes of UVB irradiation with Ga_2O_3 (0.2 gL^{-1}), In_2O_3 (0.2gL^{-1}) and TiO_2 (1.0 gL^{-1}) as catalysts.

Figure 11 - Influence of the inorganic oxidants on PFOA degradation without the presence of catalysts (0.5 g for $KBrO_3$ and 0.45 g for KIO_4) for 180 minutes of UVB irradiation.

Figure 12 – Photocatalytic degradation of PFOA with and without the addition of potassium bromate ($KBrO_3$ - 0.5 g). Results are presented after 180 minutes of UVB irradiation with the

presence of commercial and self-made Ga_2O_3 (0.2 gL^{-1}) and In_2O_3 (0.2 gL^{-1}) and commercial TiO_2 (1.0 gL^{-1}) as photocatalysts.

Table captions:

Table 1 – Particle size fractions of catalysts

Table 2 - Peak position and binding energy (BE) shift of various samples.

Table 3 - XPS results of various samples.

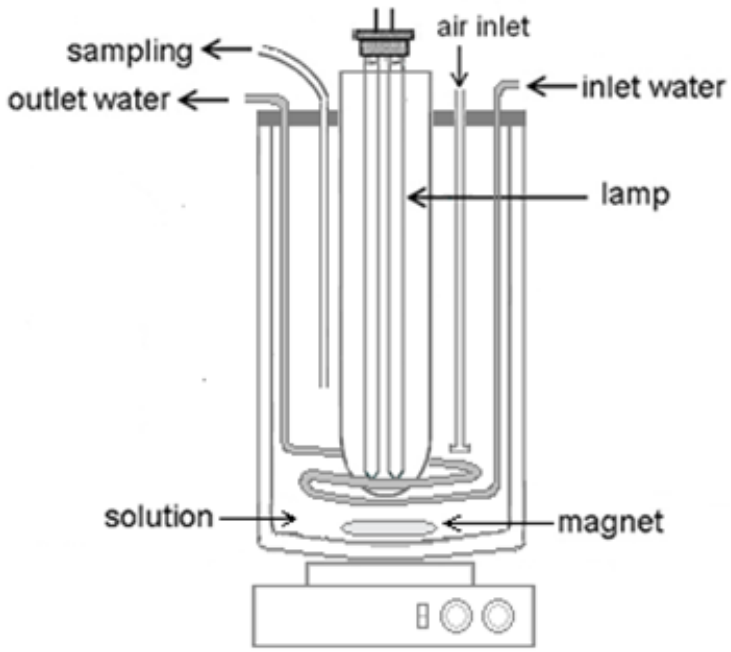
air inlet
sampling
outlet water
inlet water
lamp
solution
magnet

Figure 1

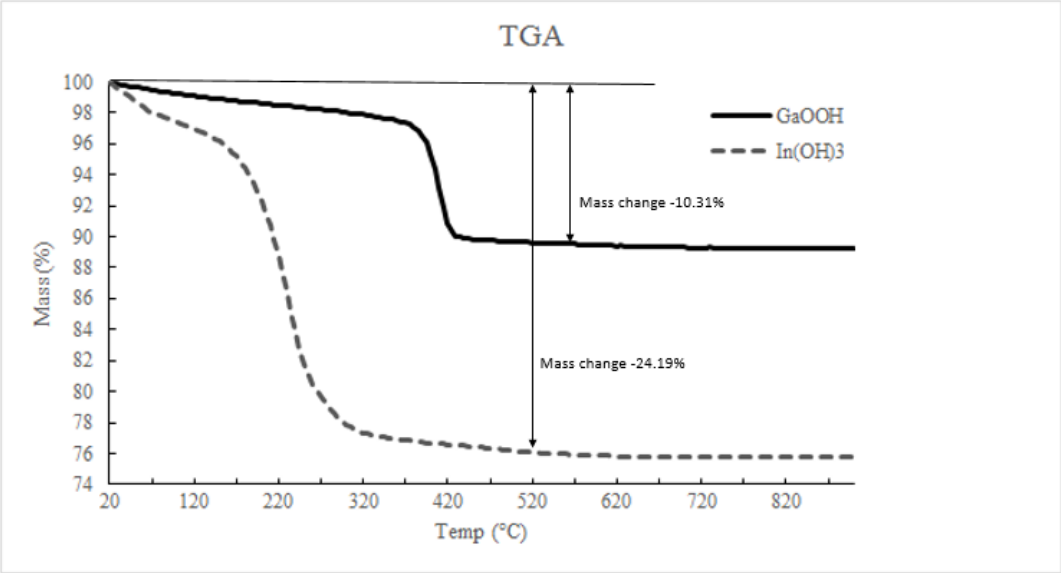
TGA
100
98
96
94
92
90
88
86
84
82
80
78
76
74
Mass (%)
20
120
220
320
420
520
620
720
820
Temp (°C)
GaOOH
In(OH)3
Mass change -10.31%
Mass change -24.19%

Figure 2

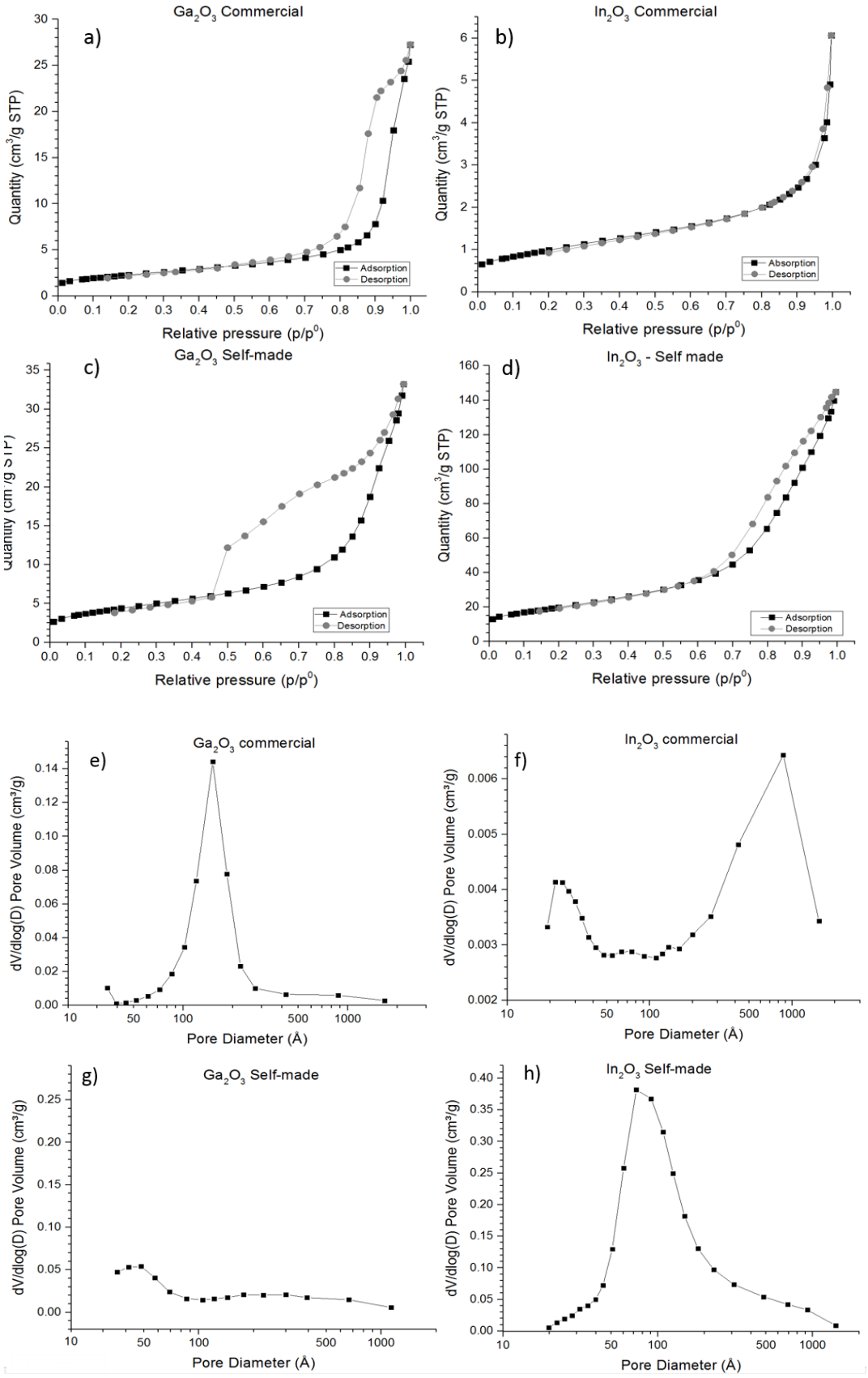
a)
Ga2O3 Commercial
Quantity (cm3/g STP)
Relative pressure (p/p0)
Adsorption
Desorption
b)
In2O3 Commercial
Quantity (cm3/g STP)
Relative pressure (p/p0)
Absorption
Desorption
c)
Ga2O3 Self-made
Relative pressure (p/p0)
Adsorption
Desorption
d)
In2O3 - Self made
Quantity (cm3/g STP)
Relative pressure (p/p0)
Adsorption
Desorption
e)
Ga2O3 commercial
dV/dlog(D) Pore Volume (cm³/g)
Pore Diameter (Å)
f)
In2O3 commercial
dV/dlog(D) Pore Volume (cm³/g)
Pore Diameter (Å)
g)
Ga2O3 Self-made
dV/dlog(D) Pore Volume (cm³/g)
Pore Diameter (Å)
h)
In2O3 Self-made
dV/dlog(D) Pore Volume (cm³/g)
Pore Diameter (Å)

Figure 3

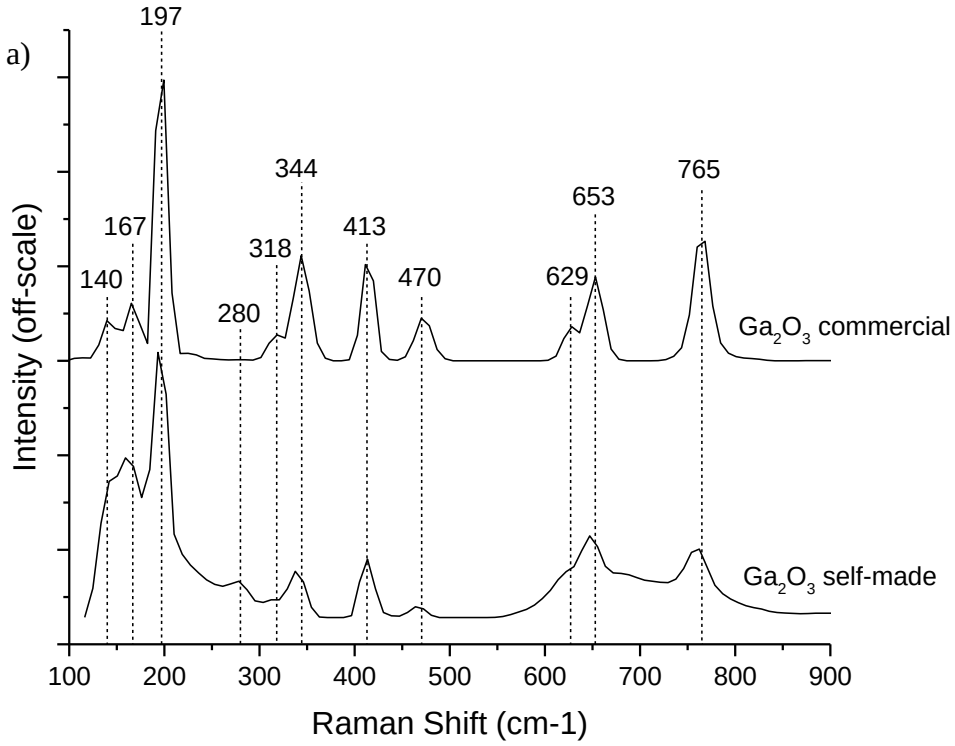

618
619

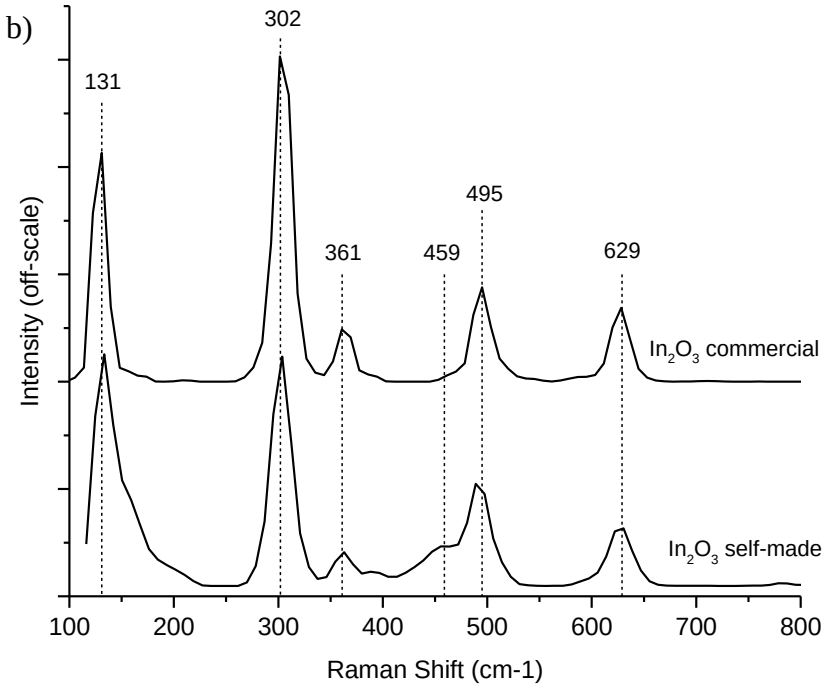

620
621 Figure 4

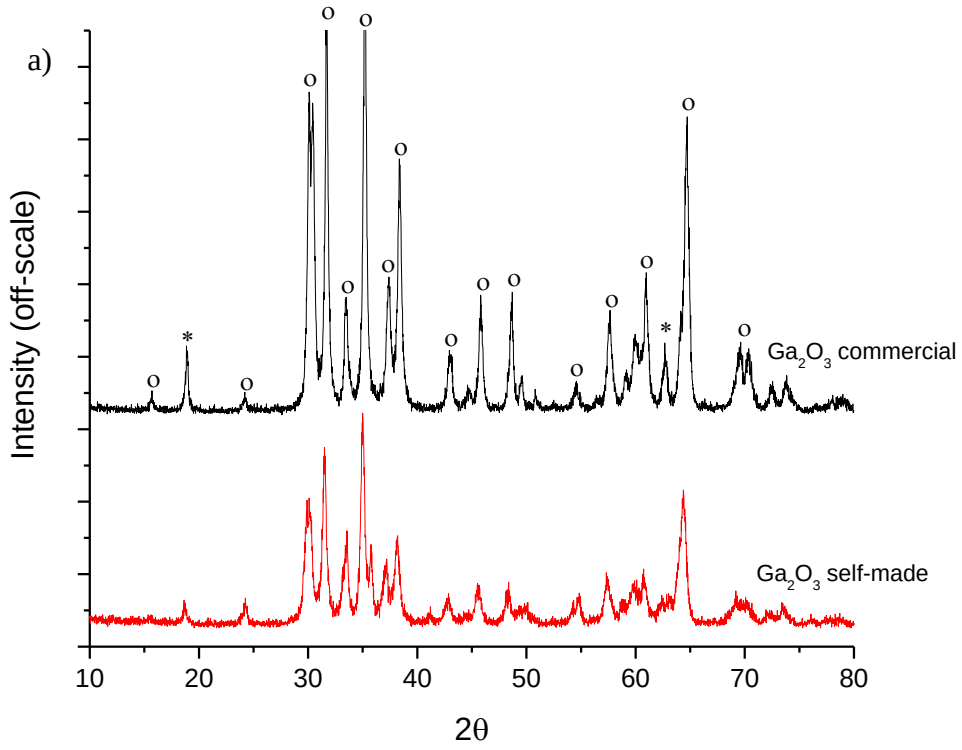

622

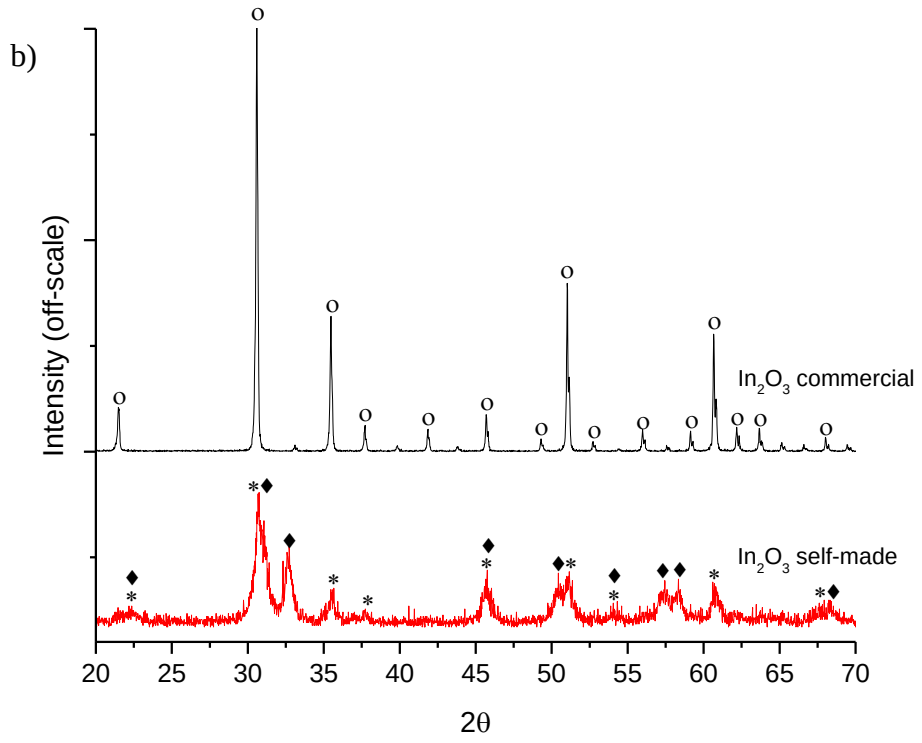

623

624 Figure 5

625

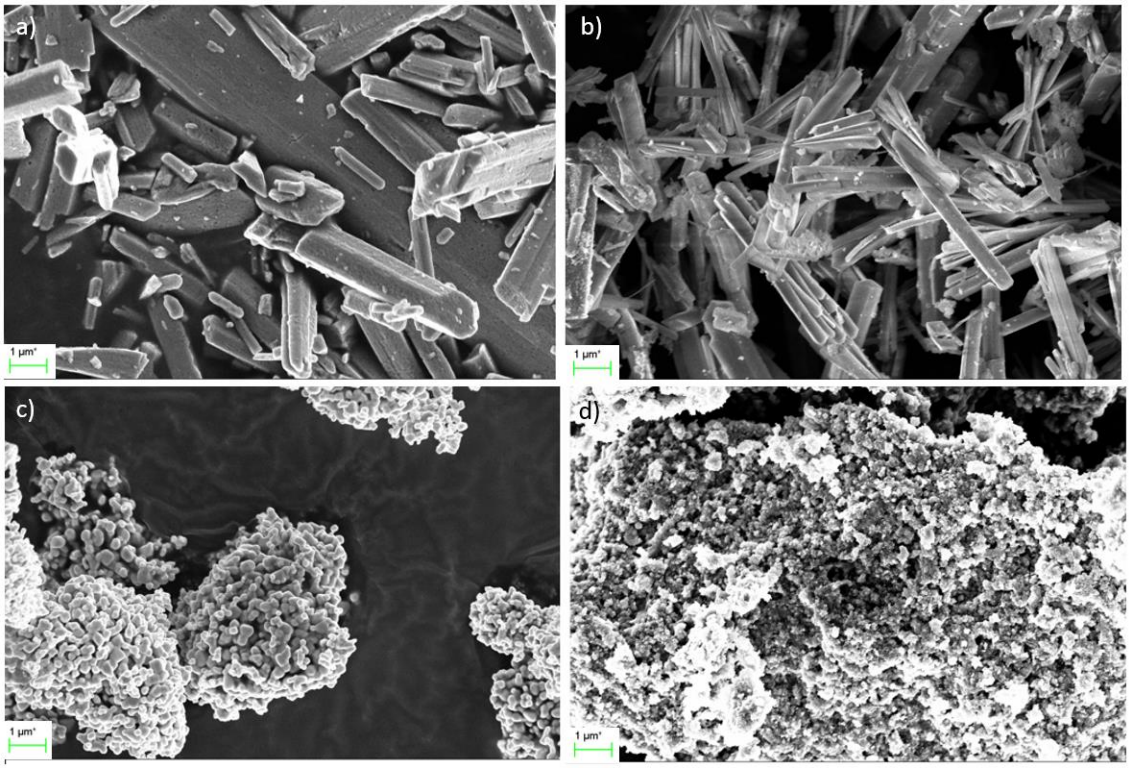

Figure 6

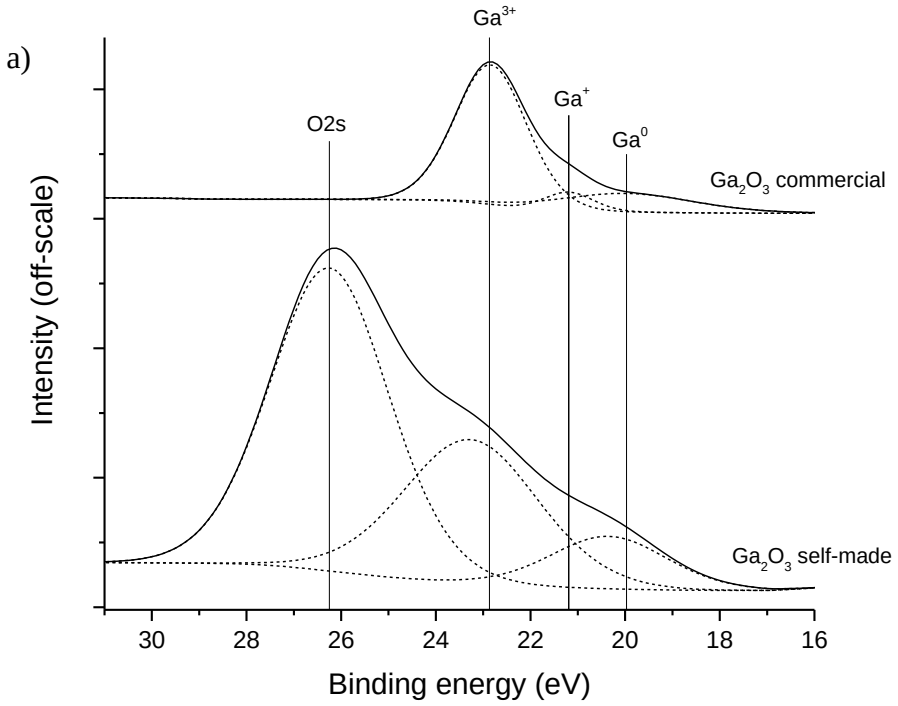

632

633

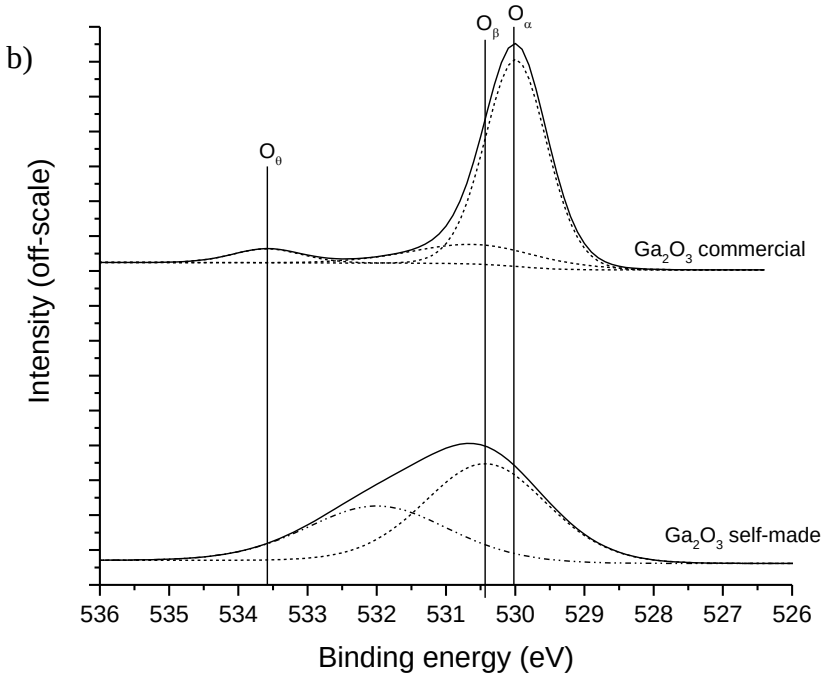

634

635

636 Figure 7

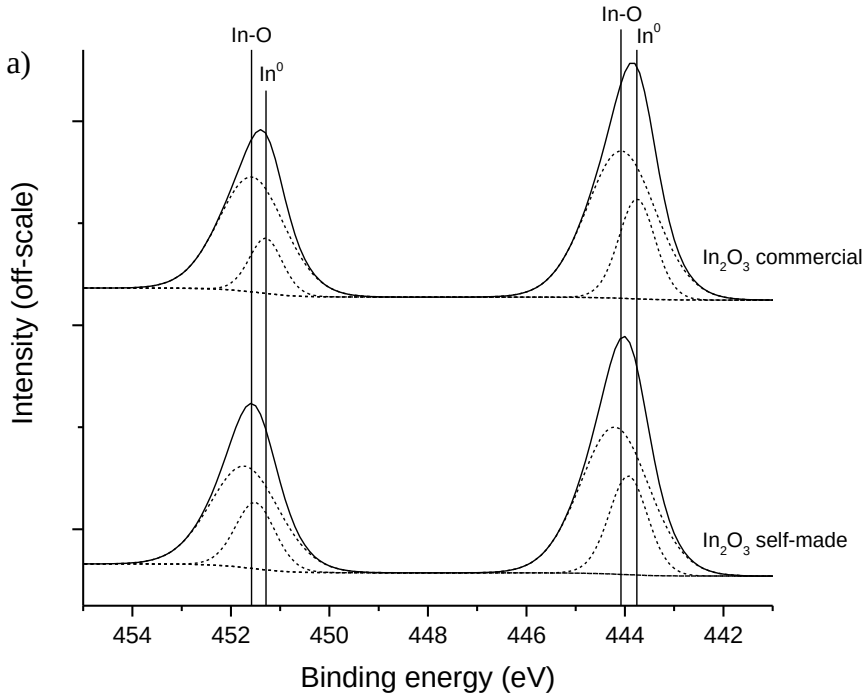

637

638

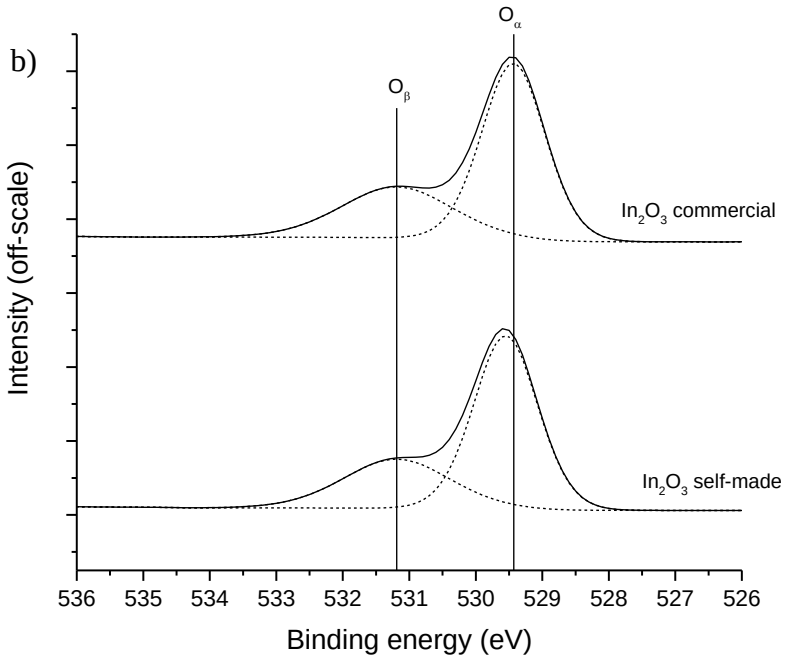

639

640

641 Figure 8

642

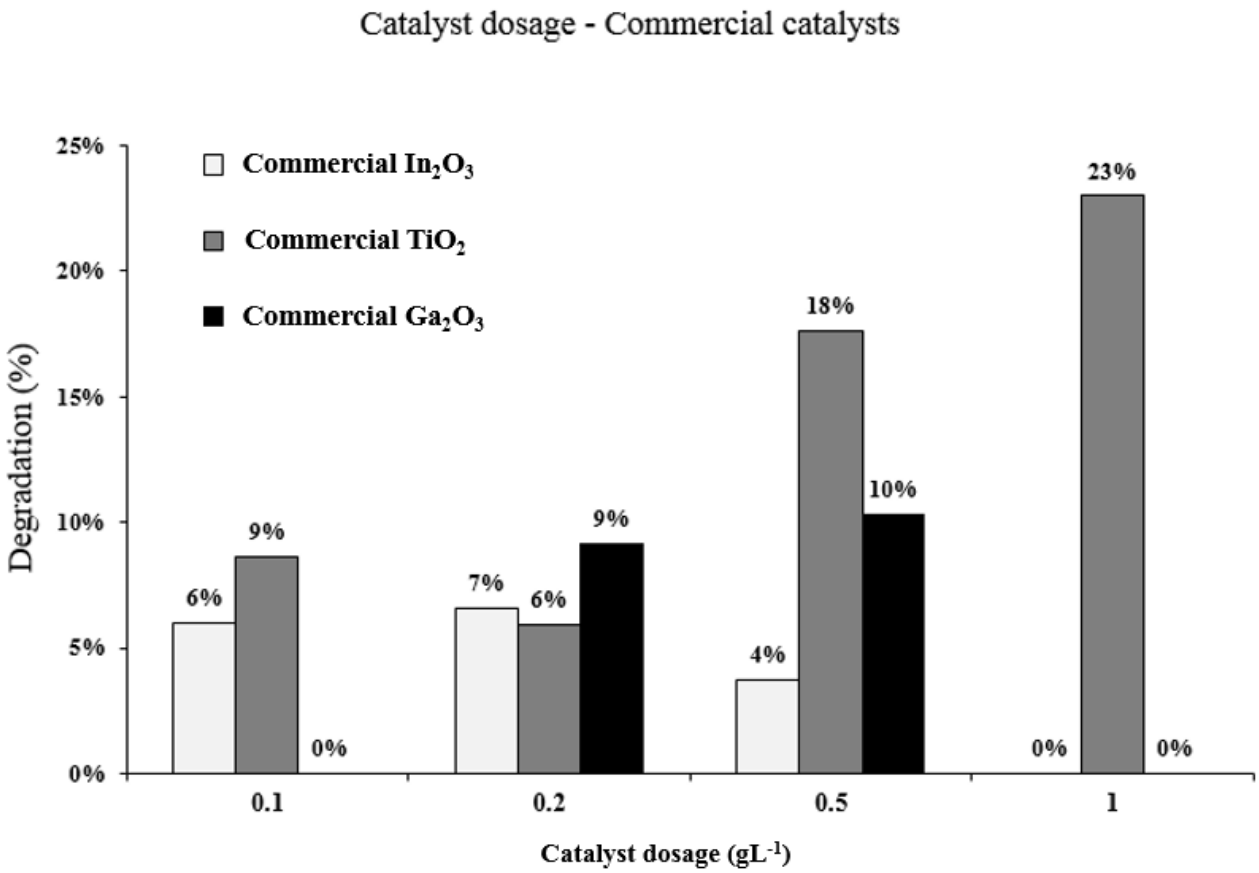
Catalyst dosage - Commercial catalysts
Commercial In_2O_3
Commercial TiO_2
Commercial Ga_2O_3
Degradation (%)
25%
20%
15%
10%
5%
0%
6%
9%
0%
7%
6%
9%
4%
18%
10%
0%
23%
0%
0.1
0.2
0.5
1
Catalyst dosage (gL^{-1})

Figure 9.

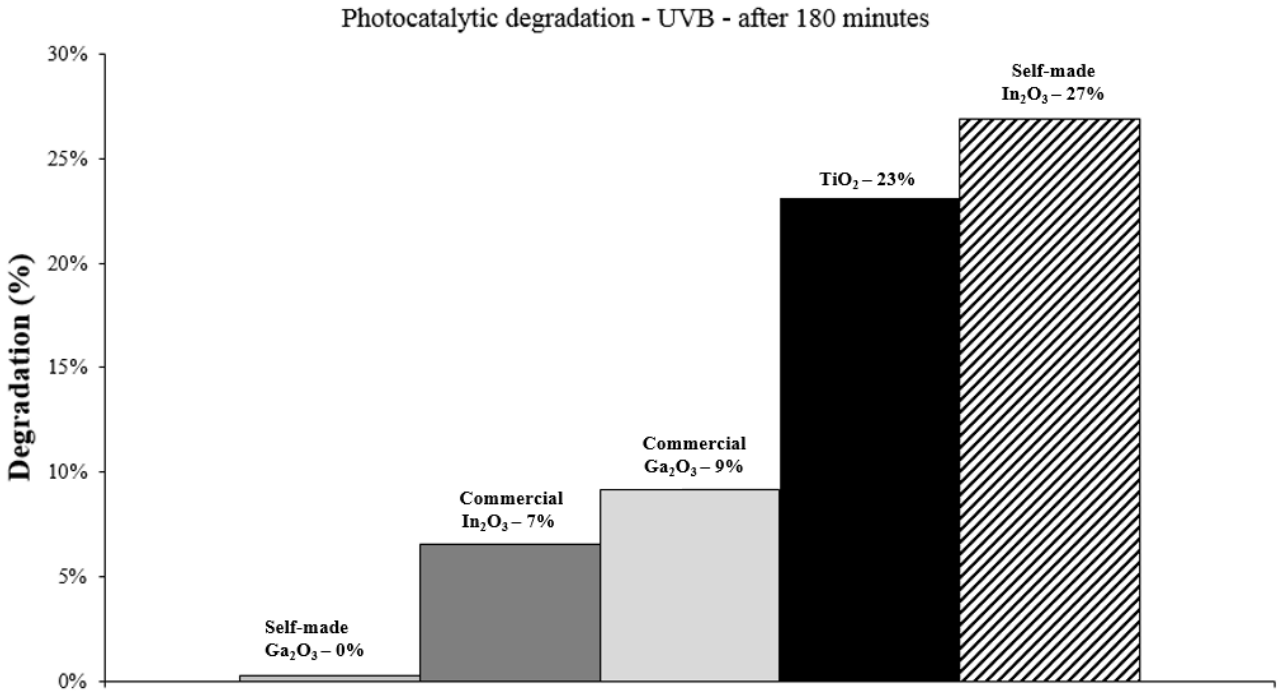
Photocatalytic degradation - UVB - after 180 minutes
Degradation (%)
30%
25%
20%
15%
10%
5%
0%
Self-made
Ga_2O_3 – 0%
Commercial
In_2O_3 – 7%
Commercial
Ga_2O_3 – 9%
TiO_2 – 23%
Self-made
In_2O_3 – 27%

Figure 10

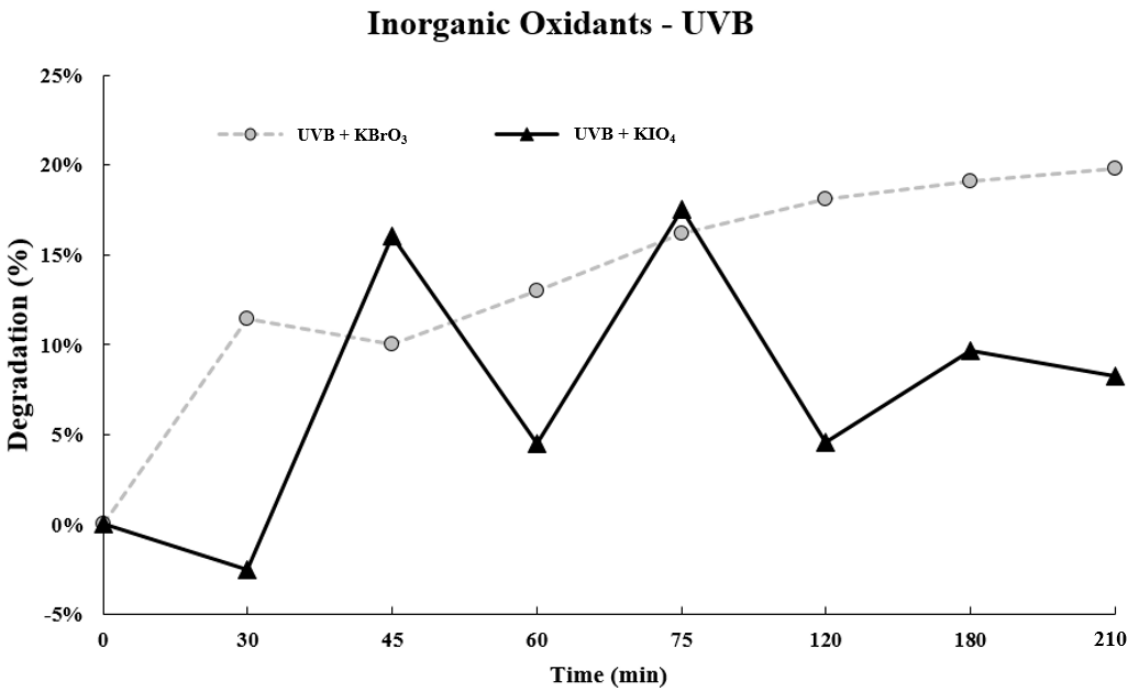
Inorganic Oxidants - UVB
25%
20%
15%
10%
5%
0%
-5%
Degradation (%)
UVB + KBrO3
UVB + KIO4
0
30
45
60
75
120
180
210
Time (min)

Figure 11

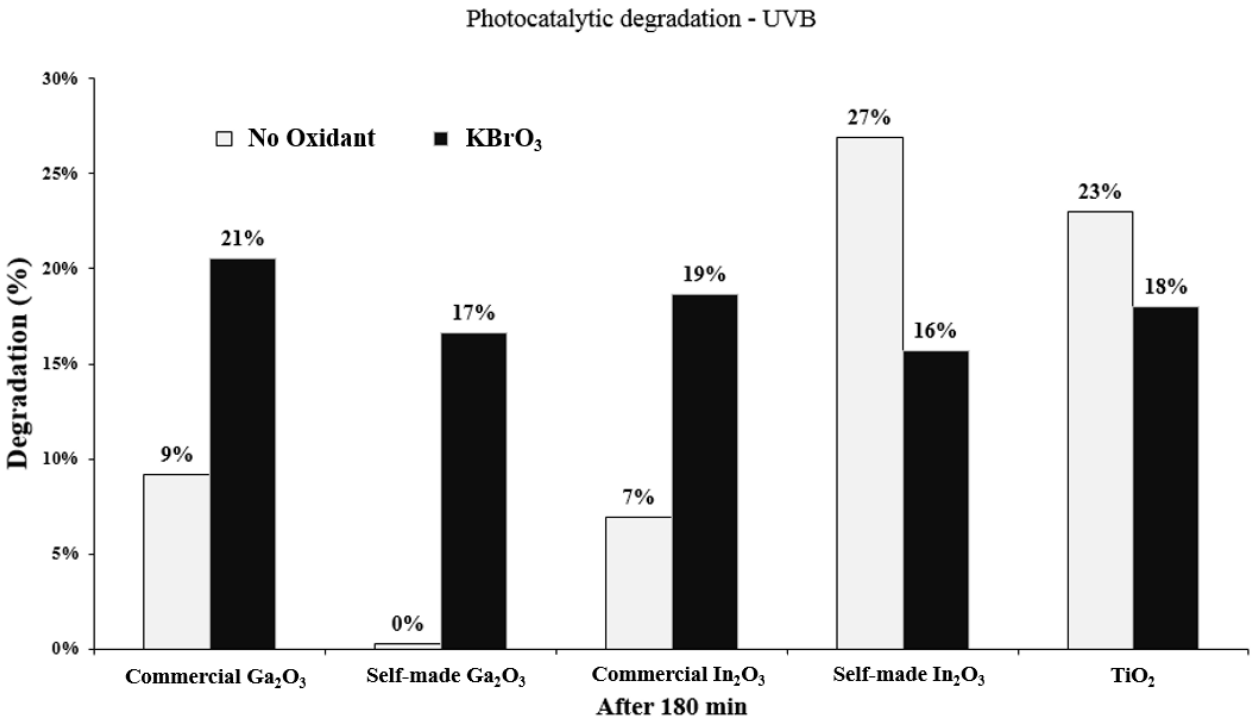
Photocatalytic degradation - UVB
No Oxidant
KBrO3
Degradation (%)
30%
25%
20%
15%
10%
5%
0%
9%
21%
0%
17%
7%
19%
27%
16%
23%
18%
Commercial Ga2O3
Self-made Ga2O3
Commercial In2O3
Self-made In2O3
TiO2
After 180 min

Figure 12

Particle-size fraction	**Ga_2O_3 Commercial**	**Ga_2O_3 self-made**	**In_2O_3 Commercial**	**In_2O_3 self-made**
> 500 µm	0 %	0 %	0 %	0 %
500 µm - 250 µm	0 %	3 %	0 %	0 %
250 µm - 100 µm	65 %	52 %	12 %	14 %
100 µm - 45 µm	34 %	45 %	23 %	43 %
< 45 µm	1 %	0 %	65 %	44 %

Table 1

	Peak BE Commercial	Peak BE Self-made	BE shift
In $3d_{5/2}$	444.08	444.21	0.13
In $3d_{3/2}$	451.58	451.72	0.14
In $3d_{5/2}$	443.76	443.93	0.17
In $3d_{3/2}$	451.29	451.51	0.22
O1s (O_α)	529.43	529.55	0.12
O1s (O_β)	531.19	531.19	0
Ga 3d (Ga^{3+})	22.84	23.27	0.43
Ga 3d (Ga^{+})	21.19	-	-
Ga 3d(Ga^{0})	19.97	20.35	0.38
O2s	-	26.25	-
O1s (O_α)	529.99	530.43	0.44
O1s (O_β)	530.58	531.99	1.41
O1s (O_θ)	533.58	-	-

Table 2

	Ga_2O_3 Commercial	Ga_2O_2 self-made	In_2O_3 Commercial	In_2O_3 Self-made
Ga^{3+} or In^{3+} [%]	74.7	76.1	76.5	72.7
O_β / (O_α+O_β+O_θ) [%]	15.3	39.1	33.5	32.0

Table 3

List of potential referees

1. Professor Simo Pehkonen, University of Eastern Finland, simo.pehkonen@uef.fi

2. Professor Sergio de Oliveira, Federal Institute of Goias, Brazil, dr_botelho@yahoo.com.br

3. Dr. Lenka Matejova, University of Ostrava, Czech Reopublic, lenka.matejova@vsb.cz